

PDF hosted at the Radboud Repository of the Radboud University Nijmegen

The following full text is a publisher's version.

For additional information about this publication click this link.

<http://hdl.handle.net/2066/92550>

Please be advised that this information was generated on 2019-06-26 and may be subject to change.

Water formation by surface O₃ hydrogenation

C. Romanzin,¹ S. Ioppolo,² H. M. Cuppen,^{2,3} E. F. van Dishoeck,^{3,4} and H. Linnartz^{2,a)}

¹LPMAA, Université Pierre et Marie Curie, Paris, France

²Sackler Laboratory for Astrophysics, Leiden Observatory, Leiden University, P.O. Box 9513, 2300 RA Leiden, The Netherlands

³Leiden Observatory, Leiden University, P.O. Box 9513, 2300 RA Leiden, The Netherlands

⁴Max-Planck-Institut für Extraterrestrische Physik, Giessenbachstrasse 1, D-85741 Garching, Germany

(Received 14 September 2010; accepted 4 December 2010; published online 24 February 2011)

Three solid state formation routes have been proposed in the past to explain the observed abundance of water in space: the hydrogenation reaction channels of atomic oxygen (O + H), molecular oxygen (O₂ + H), and ozone (O₃ + H). New data are presented here for the third scheme with a focus on the reactions O₃ + H, OH + H and OH + H₂, which were difficult to quantify in previous studies. A comprehensive set of H/D-atom addition experiments is presented for astronomically relevant temperatures. Starting from the hydrogenation/deuteration of solid O₃ ice, we find experimental evidence for H₂O/D₂O (and H₂O₂/D₂O₂) ice formation using reflection absorption infrared spectroscopy. The temperature and H/D-atom flux dependence are studied and this provides information on the mobility of ozone within the ice and possible isotope effects in the reaction scheme. The experiments show that the O₃ + H channel takes place through stages that interact with the O and O₂ hydrogenation reaction schemes. It is also found that the reaction OH + H₂ (OH + H), as an intermediate step, plays a prominent (less efficient) role. The main conclusion is that solid O₃ hydrogenation offers a potential reaction channel for the formation of water in space. Moreover, the nondetection of solid ozone in dense molecular clouds is consistent with the astrophysical picture in which O₃ + H is an efficient process under interstellar conditions. © 2011 American Institute of Physics. [doi:10.1063/1.3532087]

I. INTRODUCTION

Water is ubiquitous throughout the universe and belongs to the more abundant species in the interstellar medium. Since gas phase formation rates are not efficient at low temperatures, the formation of H₂O ice in cold dense quiescent interstellar clouds (~10 K) is expected to take place in the solid state on the surface of dust grains through H-atom addition reactions. Three different hydrogenation channels have been proposed in the past: O + H, O₂ + H, and O₃ + H.¹ Several laboratory studies investigated the formation of solid H₂O through the hydrogenation of atomic oxygen^{2,3} and molecular oxygen.⁴⁻⁹ However, only a single study¹⁰ investigated the third channel so far, showing that the deuteration of O₃ ice on an amorphous H₂O substrate leads to the formation of D₂O by detecting HDO molecules during desorption of the ice using quadrupole mass spectrometry. We give here further experimental evidence for H₂O/D₂O ice formation, presenting for the first time a comprehensive set of H/D-atom addition experiments on solid O₃ for astronomically relevant temperatures, using reflection absorption infrared spectroscopy (RAIRS).

Solid O₃ can be formed in space through energetic processing (ions, photons, and electrons) of O-bearing ices at astronomically relevant temperatures.¹¹⁻¹⁸ Tielens and Hagen¹ proposed the formation of O₃ ice through the subsequent oxidation of atomic oxygen on the surface of the interstellar grains at low temperature and in absence of UV irradiation. Ozone ice has been observed on the surface of small bodies in the solar system, such as Ganymede, Rhea, and Dione,¹⁹⁻²¹

but it has not been observed in the interstellar medium. The nondetection of solid ozone in dense molecular clouds is consistent with an efficient use-up through hydrogenation, in the case that O₃ + H is an efficient process under interstellar conditions.

Figure 1, taken from Ref. 9, shows how the three hydrogenation channels (O/O₂/O₃ + H) can interact. Specifically, the hydrogenation of solid O₃ comprises the following solid state reactions:



and



Cuppen and Herbst²² and Cazaux *et al.*²³ showed in their astrochemical models that the efficiency of this reaction channel strongly depends on the astronomical environment (e.g., diffuse clouds, dense clouds, and photon-dominated regions). Ioppolo *et al.*⁸ and Cuppen *et al.*⁹ showed experimentally that the O + H and the O₃ + H channels are connected via the O₂ + H route through common reactive intermediates (see Fig. 1). The latter channel involves the reactions



and



^{a)}Electronic mail: linnartz@strw.leidenuniv.nl.

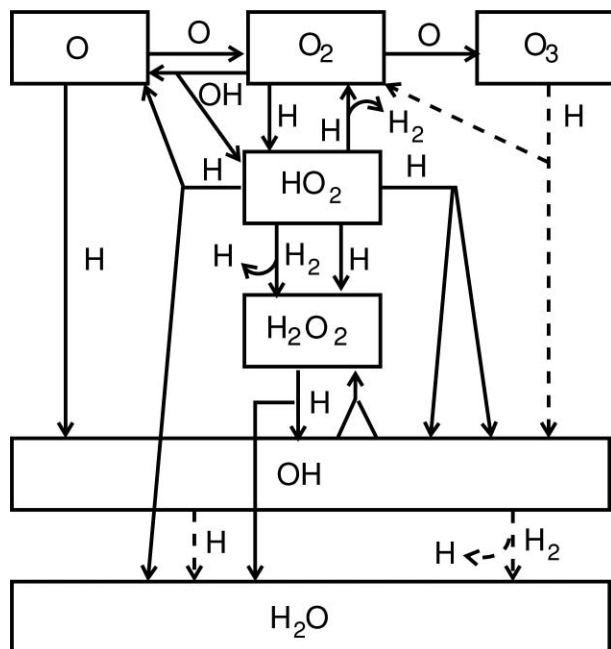


FIG. 1. A schematic representation of the water formation reaction network ($\text{O} + \text{H}$, $\text{O}_2 + \text{H}$, and $\text{O}_3 + \text{H}$). The solid arrows represent the surface reaction network as obtained from Refs. 8 and 9. The dashed arrows represent the surface reactions investigated here.

which both lead to the formation of O atoms. These can then react with O_2 to form O_3 ,



Indeed, O_3 has been found as a reaction product in hydrogenation experiments of pure O_2 ice.^{8,9}

In the following sections, we investigate the $\text{O}_3 + \text{H}$ scheme under interstellar analog conditions. We focus in particular on the first reaction step $\text{O}_3 + \text{H}$ as well as the formation of H_2O from OH through reactions (2) and (3). For this purpose, most experiments are carried out at elevated temperatures in order to instantaneously desorb the O_2 formed through reaction (1).

II. EXPERIMENTAL

The experiments are performed using an ultra high vacuum set-up, which has been described in detail elsewhere.^{8,24} It consists of an atomic beam line and a main chamber ($\sim 10^{-10}$ mbar) in which ices are grown on a cryogenically cooled (12–300 K) gold-coated copper substrate by depositing gas under an angle of 45° . A fresh O_3 sample is prepared before each experiment in a high-vacuum glass line, following the procedure as described in Ref. 25. The O_3 sample is prepared in a commercial ozone generator (Fischer-model 502, O_2 99.995% of purity, Praxair) and collected in a liquid nitrogen trap, which is used to purify the sample from O_2 pollution. O_2 deposition originating from the dissociation of O_3 in the main chamber is kept to a minimum by maintaining the substrate temperature at 40 K, well above the O_2 desorption temperature [$T_{\text{des}}(\text{O}_2) \sim 30$ K, Ref. 26]. The ice is monitored by means of RAIRS, using a Fourier transform infrared spectrometer (FTIR). The FTIR covers the range

between 4000 and 700 cm^{-1} ($2.5\text{--}14\ \mu\text{m}$) with a spectral resolution of 1 cm^{-1} . A coaddition of 256 scans yields one spectrum. RAIR difference spectra (ΔA) with respect to the deposited O_3 ice spectrum are acquired every few minutes during the hydrogenation experiment. According to Sivaraman *et al.*,¹⁸ shape and position of the $\nu_3(\text{O}_3)$ stretching mode is sensitive to the ozone environment. Therefore, the presence of other molecules should affect this infrared band, but the observed $\nu_3(\text{O}_3)$ band in our spectra after deposition is typical for a rather pure O_3 ice,^{18,27,28} instead of O_3 molecules mixed with O_2 .¹⁴

After deposition the ice is subsequently hydrogenated/deuterated at different temperatures (25, 40, and 50 K). H/D atoms are supplied by a well-characterized thermal cracking source.^{29–31} H_2/D_2 molecules are cracked in a capillary pipe surrounded by a tungsten filament, which is heated to 2200 K. During the H/D-atom exposure, the pressure in the atomic line is kept constant. Hot H/D atoms are cooled to room temperature via collisions by a nose-shaped quartz pipe, placed in the H/D-atom beam path toward the substrate. The geometry of the pipe is designed in such a way that hot species (H/D; H_2/D_2) cannot reach the ice directly (more details in Refs. 8 and 24). The H/D-atom fluxes used in our experiments are set by changing the H_2/D_2 pressure in the capillary pipe, while the filament temperature is kept constant. The final flux values (2×10^{13} and 8×10^{13} atoms $\text{cm}^{-2}\text{ s}^{-1}$ for H atoms and 1×10^{13} and 4×10^{13} atoms $\text{cm}^{-2}\text{ s}^{-1}$ for D atoms) are measured at the substrate position in the main chamber using a quadrupole mass spectrometer for the D-atom flux. The method is described in the Appendix of Ref. 8. The relative error in the D-atom flux determination is within 10%, while the relative H-atom flux determination is within 50%. The absolute error for both is estimated to be within 50%.

Several control experiments have been carried out. Deuteration experiments have been performed to estimate the maximum H_2O contamination, i.e., H_2O contributions other than those induced in the ice upon H-atom impact. This is essential as H_2O is the prime target of this study. The pollution may originate from H_2O background in the UHV setup and/or from H_2O in the high vacuum gas line. The contamination is found to increase with time and to be less ~ 1 monolayer (ML) at the end of all experiments. Results presented in Sec. IV are corrected for this contamination. In the deuteration experiments, naturally, this contamination does not play a role. Also, a pure O_3 ice has been exposed to a D_2 beam (at 40 K) to ensure that the D_2 molecules do not chemically react with the O_3 or physically change the surface through sputtering. Finally, an unprocessed O_3 ice grown at 40 K and subsequently heated to 50 K with a rate of 1 K min^{-1} shows no substantial O_3 loss because of thermal desorption [$T_{\text{des}}(\text{O}_3) \sim 63$ K, Ref. 11] over a 3 h period, the length of a typical experiment.

III. DATA ANALYSIS

After subtracting the infrared spectra with a piece-wise straight baseline, the column densities (molecules cm^{-2}) of

TABLE I. Assigned infrared features in the 4000–700 cm⁻¹ region.

Mode	Position ^a (cm ⁻¹)	Species	Position ^a (cm ⁻¹)	Species	References
libration	830	H ₂ O			32, 33
ν_3	888	H ₂ O ₂	884	D ₂ O ₂	32, 34
$\nu_2, 2\nu_4, \nu_6$	1390(*)	H ₂ O ₂	1050(*)	D ₂ O ₂	32, 34
ν_2	1650(*)	H ₂ O	1210(*)	D ₂ O	32, 33
$2\nu_6$	2840	H ₂ O ₂	2100	D ₂ O ₂	32, 34
ν_1, ν_5	3290	H ₂ O ₂	2465	D ₂ O ₂	32, 34
ν_3	3260	H ₂ O	2440	D ₂ O	32, 33
ν_3	1050	O ₃			17, 27, 35
ν_1	1107	O ₃			17, 27, 35
$\nu_1 + \nu_3$	2110	O ₃			17, 27, 35

^aAsterisks mark the features used to determine the integrated absorbance.

the newly formed species are calculated using the modified Lambert–Beer equation $N_X = \int A(\nu)d\nu/S_X$, where $A(\nu)$ is the wavelength dependent absorbance. Since literature values of transmission band strengths cannot be used directly in reflection measurements, an apparent absorption band strength, S_X of species X , is determined by individual calibration experiments. This procedure has been described in detail elsewhere (for the H₂O/D₂O and H₂O₂/D₂O₂ band strength determinations see Refs. 8 and 9). Briefly, a layer of the selected ice is deposited at a temperature lower than its desorption temperature. The sample is then linearly heated, close to its desorption temperature. Infrared spectra are acquired regularly until the desorption of the ice is complete. Such an isothermal desorption experiment has been performed to determine the apparent absorption band strength of O₃ by recording the transition from zeroth-order to first-order desorption. This is assumed to occur at the onset of the submonolayer regime and appears in the desorption curve as a sudden change in slope. The apparent absorption strength in cm⁻¹ ML⁻¹ is then calculated by relating the observed integrated area to 1 ML in the modified Lambert–Beer equation. We estimate the uncertainty of the band strength to be within 50%. The noise in the infrared spectra introduces an extra uncertainty in the H₂O/D₂O, H₂O₂/D₂O₂, and O₃ column densities, which is found to be within ± 0.5 ML for all the considered species.

The assignment of the spectral features observed in our experiments is listed in Table I. The band modes peaking at 1650/1210 cm⁻¹ (ν_2) and 1390/1050 cm⁻¹ ($\nu_2, 2\nu_4, \nu_6$) are chosen to quantify the column densities of the newly formed species upon H/D-atom exposure (solid H₂O/D₂O and H₂O₂/D₂O₂, respectively). The O₃ band peaking at 1050 cm⁻¹ (ν_3) is used to quantify the amount of O₃ deposited on the cold substrate, and, subsequently, the O₃ consumed in the surface reactions during H/D-atom addition. The 1050 cm⁻¹ D₂O₂ band overlaps with the ν_3 (O₃) band in our infrared spectra. Thus, a multi-Gaussian fit is used to separate the contributions and determine the area of the individual bands.

IV. RESULTS AND DISCUSSION

Figure 2 shows the RAIR difference spectra acquired during an hydrogenation (*left panel*) and a deuteration (*right panel*) experiment of solid O₃ at 25 K. Both H₂O/D₂O and H₂O₂/D₂O₂ integrated band intensities clearly grow as the H/D-fluence (H/D-flux \times time) increases. Neither species such as OH, HO₂, and HO₃, nor the partially deuterated species, such as HDO and HDO₂, are detected in our infrared spectra during H/D-atom addition to the O₃ ice. The presence of fully deuterated species gives experimental evidence for surface formation of water ice in the solid phase with O₃ ice as a precursor. The negative peak shown in Fig. 2 indeed reflects the O₃ use-up.

A. Temperature dependence

Figure 3 shows the H₂O/D₂O (*square*) and H₂O₂/D₂O₂ (*triangle*) column densities for the three investigated temperatures (25, 40, and 50 K) as a function of the H/D-atom fluence. The solid/open symbols correspond to the low/high H/D-atom flux used in our experiments. The amount of O₃ use-up (*circle*) during H/D-atom addition changes with the substrate temperature from ~ 1 ML at 25 K to ~ 10 ML at 50 K. This is consistent with the increase of the H/D-atom penetration depth in the O₃ ice at higher temperatures, since the mobility of O₃ molecules in the ice is expected to improve with increasing temperature, even though the penetration depth of H atoms involves only the surface of the ice and not the bulk. A similar temperature dependence has been observed for the penetration depth of H atoms in CO ice.²⁴ Another mechanism may also affect the final amount of O₃ use-up: the erosion of the ice. Each time an H/D atom reacts with an O₃ molecule through reaction (1) an O₂ molecule is formed. Whether the O₂ molecule remains on the surface of the ice

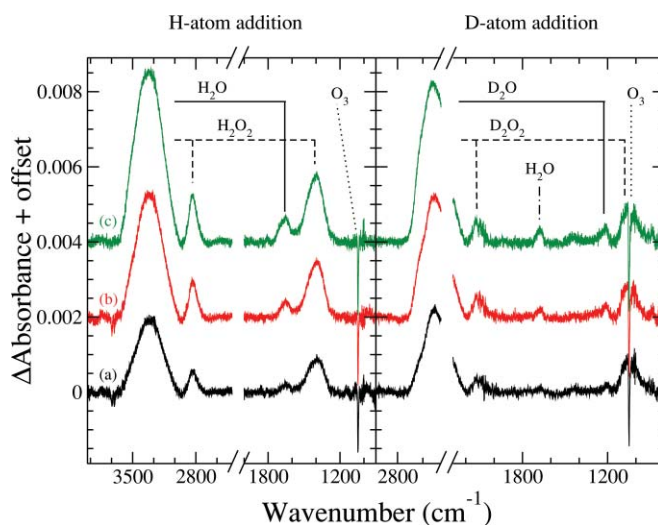


FIG. 2. Difference infrared spectra of solid O₃ ice, with respect to the spectrum before H/D-atom addition, upon hydrogenation/deuteration at 25 K for three different H/D-atom exposures: (a) 2.4×10^{16} , (b) 7.2×10^{16} , and (c) 2.0×10^{17} H/D atoms cm⁻² s⁻¹ (*left/right panel*, respectively). Spectra are offset for clarity. The water pollution is visible in the deuteration experiment (*right panel*).

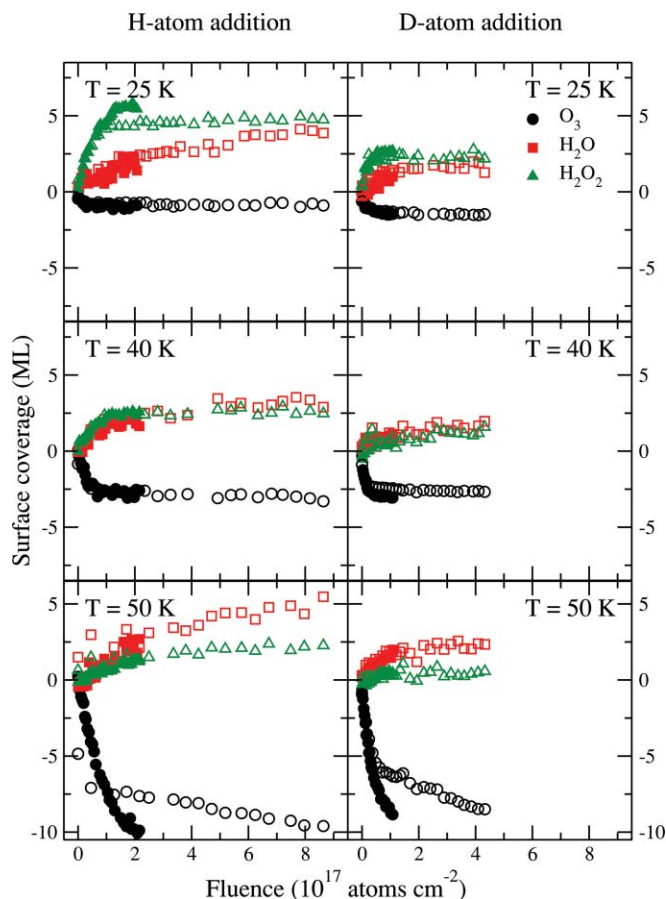


FIG. 3. Column densities for $\text{H}_2\text{O}/\text{D}_2\text{O}$ (square), $\text{H}_2\text{O}_2/\text{D}_2\text{O}_2$ (triangle), and O_3 (circle) for the three temperatures investigated (25, 40, and 50 K) as a function of the H/D-atom fluence. The hydrogenated species are plotted in the left panel, and the deuterated species in the right panel. The solid and open symbols correspond to the lower and higher H/D-atom flux (2×10^{13} and 8×10^{13} atoms $\text{cm}^{-2} \text{s}^{-1}$ for H atoms and 1×10^{13} and 4×10^{13} atoms $\text{cm}^{-2} \text{s}^{-1}$ for D atoms), respectively.

or desorbs, depends on the temperature of the ice. Below 30 K, the O_2 molecules will be further hydrogenated/deuterated according to the scheme shown in Fig. 1 (see also Refs. 8 and 9). At higher temperatures (above 30 K, see Ref. 26) the desorption of the O_2 formed through reaction (1) will leave the deeper O_3 layers exposed for H/D-atom addition, increasing the final O_3 use-up. The $\text{H}_2\text{O}/\text{D}_2\text{O}$ and $\text{H}_2\text{O}_2/\text{D}_2\text{O}_2$ column density ratios are also affected by this desorption behavior. Below 30 K, $\text{H}_2\text{O}/\text{D}_2\text{O}$ will be formed through both the hydrogenation/deuteration of O_2 ice and reactions (2) and (3). A significant amount of $\text{H}_2\text{O}_2/\text{D}_2\text{O}_2$ will be formed through the O_2 channel as well.^{8,9} For increasing temperature, the O_2 channel becomes less important and as a consequence the amount of $\text{H}_2\text{O}_2/\text{D}_2\text{O}_2$ decreases, while $\text{H}_2\text{O}/\text{D}_2\text{O}$ formation through reactions (2) and (3) becomes the dominant process.

As a side-effect of the erosion/restructuring of the ice, the H_2O pollution diluted in the O_3 ice may rearrange in islands. Consequently, the narrow H_2O bands seen after deposition of the O_3 ice in the region of the H_2O bending mode (1650 cm^{-1}) will broaden upon ice restructuring. This

effect increases with time and contributes to the total H_2O bulk feature peaking at 1650 cm^{-1} . This effect is shown in the right panel of Fig. 2. The contribution of this effect, which is estimated to be $\sim 1 \text{ ML}$ at the end of all the deuteration experiments, is taken into account for all the H-atom addition experiments, as mentioned in Sec. II.

B. H/D-atom flux dependence

Figure 3 also indicates the influence of the H/D-atom flux on the amount of reaction products. The $\text{H}_2\text{O}/\text{D}_2\text{O}$ and $\text{H}_2\text{O}_2/\text{D}_2\text{O}_2$ column densities follow the same trend for high and low H/D-atom flux and for all investigated temperatures within the experimental uncertainties. This observation is in agreement with a scenario in which a reactive system is limited only by the number of H/D atoms that reaches the ice surface. The O_3 column density follows the same behavior for high and low H/D-atom flux at temperatures below 40 K and at 50 K for a maximum H/D-atom fluence of 1×10^{16} H/D atoms cm^{-2} . However, at higher H/D-atom fluence the O_3 column density profile differs for high and low H/D-atom flux at 50 K. This is most likely caused by the transition between two different regimes: in the first regime, reaction (1) is limited by the number of H/D atoms; in the second regime, this reaction is limited by the supply of O_3 molecules, since the formed $\text{H}_2\text{O}/\text{D}_2\text{O}$ and $\text{H}_2\text{O}_2/\text{D}_2\text{O}_2$ prevent the incoming H/D atoms to reach the O_3 molecules in the lower layers. Further conversion into $\text{H}_2\text{O}/\text{D}_2\text{O}$ and $\text{H}_2\text{O}_2/\text{D}_2\text{O}_2$ is then only possible after replenishing of the top layers by fresh O_3 . This process is governed by the diffusion of O_3 in the ice, which increases with temperature and is independent of H/D-atom flux. Thus, this effect is stronger at 50 K than at 40 K and indeed the O_3 use-up follows the same trend for low and high H/D-atom fluxes when plotted as a function of exposure time instead of fluence for $> 1 \times 10^{16}$ H/D atoms cm^{-2} . The two regimes are schematically depicted in Fig. 4.

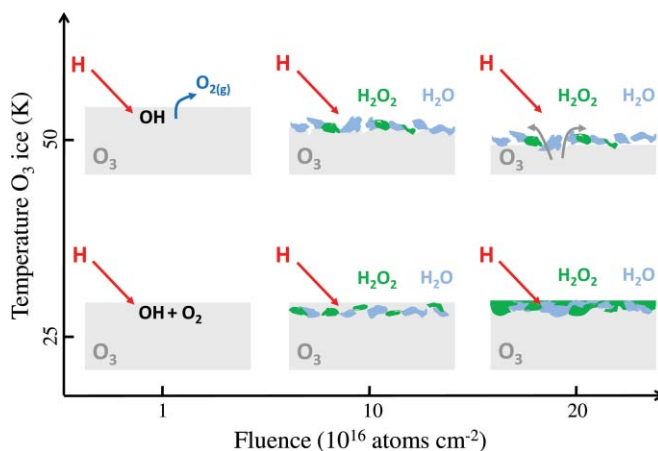


FIG. 4. Schematic representation of the hydrogenation of O_3 ice as a function of the temperature and H-atom fluence: at temperatures below 40 K (bottom) reaction (1) is limited by the number of H/D atoms, at higher temperatures (top) this reaction is limited by the supply of O_3 molecules. The replenishing of the top layers is induced by diffusion of O_3 in the ice. The erosion of the ice at 50 K is also shown (top).

TABLE II. Amounts of O₃ use-up, and formed H₂O/D₂O and H₂O₂/D₂O₂ in ML after an exposure of 1.1×10^{17} H/D atoms cm⁻² and 4.2×10^{17} H/D atoms cm⁻² (low and high fluxes, respectively) at the three different substrate temperatures investigated. See Sec. III for the determination of the values and the corresponding errors. The O_{budget} corresponds to the mass-balance of O atoms in ML: O_{budget} = -3O₃ + H₂O + 2H₂O₂, or the equivalent for deuteration.

H/D-flux (cm ⁻² s ⁻¹)	T (K)	O ₃ (ML)	H ₂ O (ML)	H ₂ O ₂ (ML)	O _{budget} (ML)	O ₃ (ML)	D ₂ O (ML)	D ₂ O ₂ (ML)	O _{budget} (ML)
$2/1 \times 10^{13}$	25	0.8	1.5	4.9	8.9	1.5	1.0	2.7	1.9
	40	2.7	1.8	2.3	-1.7	3.0	1.1	0.6	-6.7
	50	7.4	1.2	0.7	-19.6	8.8	1.8	0.5	-23.6
$8/4 \times 10^{13}$	25	0.8	3.1	4.6	9.9	1.5	1.6	2.2	1.5
	40	2.9	2.9	2.6	-0.6	2.7	1.6	1.4	-3.7
	50	8.1	3.7	1.8	-17.0	8.5	2.2	0.5	-22.3

C. Possible reaction pathways

The investigation of the mass balance between the formed and consumed species in our ice after H/D-atom addition allows identifying the most likely reaction channel responsible for the formation of solid H₂O ice. The mass balance for oxygen atoms can be determined looking at the number of O atoms present in each species (O_{budget} = -3O₃ + H₂O + 2H₂O₂). From the comparison of the results listed in Table II, we summarize three relevant results: (i) the O atoms are found in excess only at 25 K (O_{budget} = 9.9/8.9 ML for higher/lower H-atom flux and 1.5/1.9 ML for both higher/lower D-atom flux); (ii) part of the O use-up is not converted into H₂O/D₂O and H₂O₂/D₂O₂ at 40 and 50 K (negative O_{budget}); and (iii) there appears to be a strong isotope effect in the formation of H₂O/D₂O and H₂O₂/D₂O₂ (more H₂O and H₂O₂ than D₂O and D₂O₂).

Point (i) can be explained by the presence of an extra O₂ poisoning layer deposited on top of the O₃ ice at 25 K. The extra O₂ originates from background deposition, while the substrate was cooled from 40 to 25 K with a rate of 1 K min⁻¹. This effect is already minimized by lowering the surface temperature only after the main chamber pressure has substantially dropped toward the standard value of 10⁻¹⁰ mbar. However, the deposition of a maximum of 5 ML of O₂ on top of the O₃ ice cannot be prevented for the 25 K experiments

(5 ML of O₂ correspond to 10 ML of O atoms). The higher value for the O_{budget} in the 25 K hydrogenation experiment with respect to the deuteration experiment is consistent with a higher penetration depth of H atoms in the O₂ ice compared to D atoms.⁵

Point (ii) is addressed by the fact that most of the O₂ produced through reaction (1) is lost at temperatures higher than the O₂ ice desorption temperature. OH/OD and H₂O/D₂O can desorb upon reaction as well. We will discuss this issue in more detail in the next paragraph, which deals with point (iii).

Roughly the same amount of O₃ is used-up for the hydrogenation and deuteration experiments. This indicates that the observed isotope effect [point (iii)] is not due to a different rate for hydrogenation and deuteration of O₃, but that it is probably caused by a different desorption probability upon reaction. Table II suggests that D₂O and D₂O₂ are more likely to desorb than H₂O and H₂O₂. Thermal desorption, however, would lead to the reverse and therefore this effect has to come from the reaction energetics. We will first consider H₂O/D₂O, which is formed in two steps. In the first step, reaction (1), most of the excess energy will be released in the form of ro-vibrational excitation of OH/OD or in translational energy. Gas phase calculations show that this translational energy is 5.4% higher for deuteration than for hydrogenation,³⁶ which would lead to a slightly higher desorption probability for D + O₃ than for H + O₃ and may explain at least part of the observed effect. If H₂O/D₂O is then mainly formed from OH/OD through reaction (2) (see left side of Fig. 5), the large overall difference in desorption probability still cannot be fully explained. It can however be explained if H₂O/D₂O is mainly formed through reaction (3). In order to conserve momentum, the kinetic energy is distributed over the products according to the inverse mass. This means that D₂O will have nearly twice the kinetic energy of H₂O after reaction (3) ($E_{D_2O}/E_D = 2/20$ and $E_{H_2O}/E_H = 1/18$). Since the total excess energy of ~ 1 eV is close to the desorption energy of H₂O (0.9 eV, Ref. 37), this difference in kinetic energy will have a substantial effect on the desorption probability. Therefore, in this case more D₂O will desorb from the ice.

The observed isotope effect for H₂O/D₂O can thus be explained by reaction (3) instead of reaction (2). On first glance one would however expect reaction (2) to be more efficient than reaction (3), since the first is barrierless with an excess

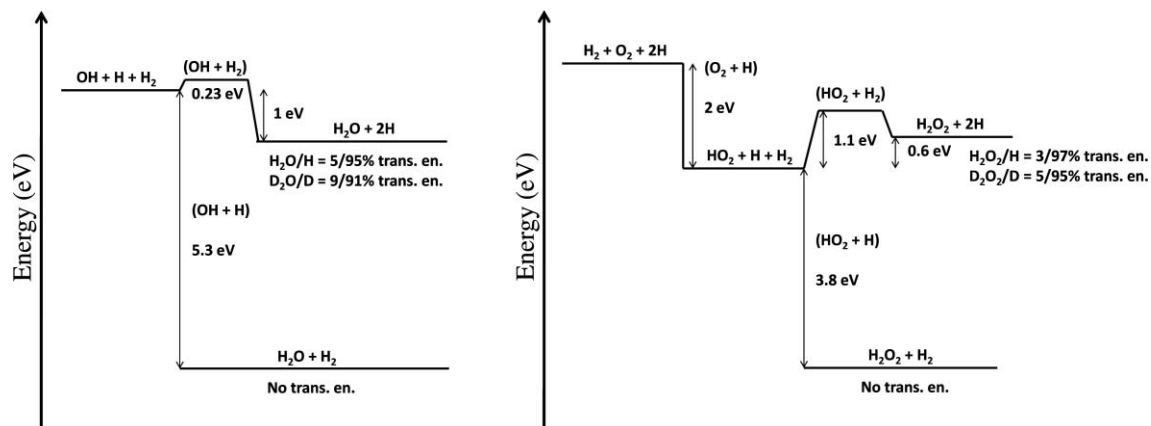


FIG. 5. Proposed reaction mechanism for the formation of H₂O (left side) and H₂O₂ (right side) from hydrogenation of O₃ ice. Reactions are shown in brackets.

of 5.3 eV, and the second has a barrier of 0.234 eV (Ref. 38) with an excess of 1 eV. The problem with reaction (2) is that one needs to dissipate 5.3 eV of excess energy with just one product. Part of this could be absorbed by the ice surface, but the weak interactions between the product and the ice limits the full dissipation. A reaction where only 1 eV of excess energy is released over two products is therefore more likely, especially since H₂ is abundantly present in our experiment, because the H-atom beam entering the main chamber contains a large fraction of cold H₂.

Furthermore, gas phase experiments indicate that tunneling becomes important for OH + H₂ below 250 K. The reaction rate at 25–50 K will therefore be substantially increased through tunneling. This also leads to an extra isotope effect where OH + H₂ has probably a higher rate than D₂ + OD. In addition, OH/OD is formed “hot” and this energy can also be used to overcome the reaction barrier. Reaction (3) may therefore be more relevant than reaction (2). These two reactions were previously included in the complete reaction network for O₂ surface hydrogenation investigated in Ref. 9, although no experimental evidence was found for reaction (3). However, the method used there was not very sensitive to the detection of this particular reaction. Therefore, extra dedicated studies specifically on the OH + H₂ reaction are needed to determine the absolute efficiency of this reaction, especially in light of the present study, which indicates that this reaction may be crucial as a final step in all three water formation channels (O/O₂/O₃ + H).

Similar arguments can be used for the formation of H₂O₂/D₂O₂ from HO₂/DO₂ by



or



where the latter can again lead to an isotope effect with more D₂O₂ than H₂O₂ desorption and a lower rate of reaction for D₂ + DO₂ through tunneling (see right side of Fig. 5). HO₂ + H₂ has a high barrier of 1.1 eV and is endothermic by –0.6 eV. However, in the aforementioned study we have observed this reaction to proceed.⁹ The exothermicity of O₂ + H may help to overcome the barrier and the endothermicity, since the total reaction



composed of



and



is exothermic by 1.3 eV.

To summarize, the observed isotope effect between H₂O/H₂O₂ and D₂O/D₂O₂ in the O₃ hydrogenation channel can be explained by a combination of effects. First, OD will get more translational energy than OH in reaction (1). Then, if H₂O₂ and H₂O are formed through reactions with H₂, tunneling leads to a higher rate for hydrogenation than deuteration, and second, the distribution of excess energy can

lead to more D₂O/D₂O₂ than H₂O/H₂O₂ desorption. O₃ is destroyed equally for H and D, which indicates that reaction (1) proceeds without substantial tunneling effect.

Finally, all the experimental results discussed here, i.e., points (i), (ii), and (iii), are obtained under laboratory conditions, and consequently some parameters necessarily differ orders of magnitude from those typical for interstellar conditions, i.e., the time scale to reach a comparable H-atom fluence. More critically, the use of excess energy to allow further reaction steps in the laboratory may be absent under astronomical conditions. The excess energy of the OH radical formed through reaction (1), for example, may be dissipated in the ice before H₂ would reach this radical on an interstellar timescale. However, a two step reaction mechanism may still apply to the interstellar medium at low temperature (10 K), if an H₂ layer is available on the surface of the ice for further reactions. However, the differences between laboratory and interstellar conditions do not change the main conclusion of the work presented here: water is formed efficiently at low temperatures through hydrogenation of O₃ ice and reaction (3) may be more relevant than reaction (2) under interstellar ice analog conditions.

V. CONCLUSION

The present study shows that the water formation through hydrogenation of solid O₃ ice as proposed by Tielens and Hagen¹ takes place under interstellar ice analog conditions. Hydrogenation of O₃ ice exhibits a similar temperature dependency as seen for CO ice:²⁴ the mobility of O₃ molecules increases with the temperature, while the penetration depth of H atoms into the ice involves only the first monolayers. For temperatures above the O₂ desorption temperature, hydrogenation of O₃ leads to erosion of the ice, since O₂ formed in the reaction O₃ + H desorbs. The remaining OH can further react to H₂O and H₂O₂. The erosion occurs until a layer of H₂O and H₂O₂ layer covers the ice and prevents the incoming H atoms from reaching the underlying O₃ ice. It is found that at high surface temperature (50 K) O₃ is mobile enough to slowly diffuse through the H₂O and H₂O₂ layer and to become available for further hydrogenation on the surface of the ice.

Experimental evidence is found for the connection of the O₃ hydrogenation channel to the O + H and O₂ + H channels, as summarized in Fig. 1. As a result it has become possible to draw conclusions on several reactions that are part of the other two hydrogenation channels. The results indicate that the reaction OH + H₂ is most likely more efficient than the reaction OH + H: reaction OH + H₂ could proceed through tunneling, while reaction OH + H needs to dissipate 5.3 eV of excess energy with just one product, which could be difficult. Our experimental results complete the reaction scheme initially proposed in Ref. 1 to explain surface water formation in space. The conclusion that the three channels (O/O₂/O₃ + H) are strongly linked is of importance for astrochemical models focusing on water formation under interstellar conditions.

ACKNOWLEDGMENTS

We thank M. van Hemert, T. P. M. Goumans, C. Arasa, E. Fayolle and K. I. Öberg for stimulating and fruitful discussions, and G. Schwaab (University of Bochum) for providing the ozone generator. The research leading to these results has received funding from NOVA, the Netherlands Research School for Astronomy, a Spinoza grant from the Netherlands Organization for Scientific Research, NWO, and the European Community's Seventh Framework Programme (FP7/2007-2013) under Grant Agreement No. 238258.

- ¹A. G. G. M. Tielens and W. Hagen, *Astron. Astrophys.* **114**, 245 (1982).
- ²K. Hiraoka, T. Miyagoshi, T. Takayama, K. Yamamoto, and Y. Kihara, *Astrophys. J.* **498**, 710 (1998).
- ³F. Dulieu, L. Amiaud, E. Congiu, J. Fillion, E. Matar, A. Momeni, V. Pirronello, and J. L. Lemaire, *Astron. Astrophys.* **512**, A30 (2010).
- ⁴N. Miyauchi, H. Hidaka, T. Chigai, A. Nagaoka, N. Watanabe, and A. Kouchi, *Chem. Phys. Lett.* **456**, 27 (2008).
- ⁵S. Ioppolo, H. M. Cuppen, C. Romanzin, E. F. van Dishoeck, and H. Linnartz, *Astrophys. J.* **686**, 1474 (2008).
- ⁶E. Matar, E. Congiu, F. Dulieu, A. Momeni, and J. L. Lemaire, *Astron. Astrophys.* **492**, L17 (2008).
- ⁷Y. Oba, N. Miyauchi, H. Hidaka, T. Chigai, N. Watanabe, and A. Kouchi, *Astrophys. J.* **701**, 464 (2009).
- ⁸S. Ioppolo, H. M. Cuppen, C. Romanzin, E. F. van Dishoeck, and H. Linnartz, *Phys. Chem. Chem. Phys.* **12**, 12065 (2010).
- ⁹H. M. Cuppen, S. Ioppolo, C. Romanzin, and H. Linnartz, *Phys. Chem. Chem. Phys.* **12**, 12077 (2010).
- ¹⁰H. Mokrane, H. Chaabouni, M. Accolla, E. Congiu, F. Dulieu, M. Chehrouri, and J. L. Lemaire, *Astrophys. J. Lett.* **705**, L195 (2009).
- ¹¹M. Famá, D. A. Bahr, B. D. Teolis, and R. A. Baragiola, *Nucl. Instrum. Methods Phys. Res. B* **193**, 775 (2002).
- ¹²M. J. Loeffler, U. Raut, R. A. Vidal, R. A. Baragiola, and R. W. Carlson, *Icarus* **180**, 265 (2006).
- ¹³P. D. Cooper, M. H. Moore, and R. L. Hudson, *Icarus* **194**, 379 (2008).
- ¹⁴L. Schriver-Mazzuoli, A. de Saxcé, C. Lugez, C. Camy-Peyret, and A. Schriver, *J. Chem. Phys.* **102**, 690 (1995).
- ¹⁵P. A. Gerakines, W. A. Schutte, and P. Ehrenfreund, *Astron. Astrophys.* **312**, 289 (1996).
- ¹⁶S. Lacombe, F. Cemic, K. Jacobi, M. N. Hedhili, Y. Le Coat, R. Azria, and M. Tronc, *Phys. Rev. Lett.* **79**, 1146 (1997).
- ¹⁷C. J. Bennett and R. I. Kaiser, *Astrophys. J.* **635**, 1362 (2005).
- ¹⁸B. Sivaraman, C. S. Jamieson, N. J. Mason, and R. I. Kaiser, *Astrophys. J.* **669**, 1414 (2007).
- ¹⁹K. S. Noll, R. E. Johnson, A. L. Lane, D. L. Domingue, and H. A. Weaver, *Science* **273**, 341 (1996).
- ²⁰K. S. Noll, T. L. Roush, D. P. Cruikshank, R. E. Johnson, and Y. J. Pendleton, *Nature (London)* **388**, 45 (1997).
- ²¹A. R. Hendrix, C. A. Barth, and C. W. Hord, *J. Geophys. Res.* **104**, 14169 (1999).
- ²²H. M. Cuppen and E. Herbst, *Astrophys. J.* **668**, 294 (2007).
- ²³S. Cazaux, V. Cobut, M. Marseille, M. Spaans, and P. Caselli, *Astron. Astrophys.* **522**, A74 (2010).
- ²⁴G. W. Fuchs, H. M. Cuppen, S. Ioppolo, S. E. Bisschop, S. Andersson, E. F. van Dishoeck, and H. Linnartz, *Astron. Astrophys.* **505**, 629 (2009).
- ²⁵D. D. Berkley, B. R. Johnson, N. Anand, K. M. Beauchamp, and L. E. Conroy, *Appl. Phys. Lett.* **53**, 1973 (1988).
- ²⁶K. Acharyya, G. W. Fuchs, H. J. Fraser, E. F. van Dishoeck, and H. Linnartz, *Astron. Astrophys.* **466**, 1005 (2007).
- ²⁷H. Chaabouni, L. Schriver-Mazzuoli, and A. Schriver, *Low Temp. Phys.* **26**, 712 (2000).
- ²⁸E. Y. Misochko, A. V. Akimov, and C. A. Wight, *J. Phys. Chem. A* **103**, 7972 (1999).
- ²⁹K. G. Tschersich and V. von Bonin, *J. Appl. Phys.* **84**, 4065 (1998).
- ³⁰K. G. Tschersich, *J. Appl. Phys.* **87**, 2565 (2000).
- ³¹K. G. Tschersich, J. P. Fleischhauer, and H. Schuler, *J. Appl. Phys.* **104**, 034908 (2008).
- ³²P. A. Giguère and K. B. Harvey, *J. Mol. Spectrosc.* **3**, 36 (1959).
- ³³D. F. Hornig, H. F. White, and F. P. Reding, *Spectrochim. Acta* **12**, 338 (1958).
- ³⁴J. A. Lannon, F. D. Verderame, and R. W. Anderson, Jr., *J. Chem. Phys.* **54**, 2212 (1971).
- ³⁵P. Brosset, R. Dahoo, B. Gauthierroy, L. Abouafmarguin, and A. Lakhlifi, *Chem. Phys.* **172**, 315 (1993).
- ³⁶H. G. Yu and A. J. C. Varandas, *J. Chem. Soc., Faraday Trans.* **93**, 2651 (1997).
- ³⁷S. Andersson, A. Al-Halabi, G. Kroes, and E. F. van Dishoeck, *J. Chem. Phys.* **124**, 064715 (2006).
- ³⁸M. Yang, D. H. Zhang, M. A. Collins, and S. Lee, *J. Chem. Phys.* **115**, 174 (2001).